

Well-Established Nucleon Resonances Revisited by Double-Polarization Measurements

A. Thiel,¹ A. V. Anisovich,^{1,2} D. Bayadilov,^{1,2} B. Bantes,³ R. Beck,¹ Yu. Beloglazov,^{1,2} M. Bichow,⁴ S. Böse,¹ K.-Th. Brinkmann,^{1,5} Th. Challand,⁶ V. Crede,⁷ F. Dietz,⁵ P. Drexler,⁵ H. Dutz,³ H. Eberhardt,³ D. Elsner,³ R. Ewald,³ K. Fornet-Ponse,³ St. Friedrich,⁵ F. Frommberger,³ Ch. Funke,¹ M. Gottschall,¹ M. Grüner,¹ E. Gutz,¹ Ch. Hammann,¹ J. Hannappel,³ J. Hartmann,¹ W. Hillert,³ Ph. Hoffmeister,¹ Ch. Honisch,¹ I. Jaegle,⁶ I. Jürgensen,¹ D. Kaiser,¹ H. Kalinowsky,¹ F. Kalischewski,¹ S. Kammer,³ I. Keshelashvili,⁶ V. Kleber,³ F. Klein,³ E. Klempt,¹ B. Krusche,⁶ M. Lang,¹ I. Lopatin,² Y. Maghrbi,⁶ K. Makonyi,⁵ V. Metag,⁵ W. Meyer,⁴ J. Müller,¹ M. Nanova,⁵ V. Nikonov,^{1,2} R. Novotny,⁵ D. Piontek,¹ G. Reicherz,⁴ A. Sarantsev,^{1,2} Ch. Schmidt,¹ H. Schmieden,³ T. Seifen,¹ V. Sokhoyan,¹ V. Sumachev,² U. Thoma,¹ H. vanPee,¹ D. Walther,¹ Ch. Wendel,¹ U. Wiedner,⁴ A. Wilson,⁷ A. Winnebeck,¹ and Y. Wunderlich¹

(CBELSA/TAPS Collaboration)

¹*Helmholtz–Institut für Strahlen– und Kernphysik, Universität Bonn, Germany*

²*Petersburg Nuclear Physics Institute, Gatchina, Russia*

³*Physikalisches Institut, Universität Bonn, Germany*

⁴*Institut für Experimentalphysik I, Universität Bochum, Germany*

⁵*II. Physikalisches Institut, Universität Gießen, Germany*

⁶*Physikalisches Institut, Universität Basel, Switzerland*

⁷*Department of Physics, Florida State University, Tallahassee, Florida 32306-4350, USA*

(Received 11 May 2012; published 5 September 2012)

The first measurement is reported of the double-polarization observable G in the photoproduction of neutral pions off protons, covering the photon energy range from 620 to 1120 MeV and the full solid angle. G describes the correlation between the photon polarization plane and the scattering plane for protons polarized along the direction of the incoming photon. The observable is highly sensitive to contributions from baryon resonances. The new results are compared to the predictions from SAID, MAID, and BnGa partial wave analyses. In spite of the long-lasting efforts to understand $\gamma p \rightarrow p\pi^0$ as the simplest photoproduction reaction, surprisingly large differences between the new data and the latest predictions are observed which are traced to different contributions of the $N(1535)$ resonance with spin parity $J^P = 1/2^-$ and $N(1520)$ with $J^P = 3/2^-$. In the third resonance region, where $N(1680)$ with $J^P = 5/2^+$ production dominates, the new data are reasonably close to the predictions.

DOI: [10.1103/PhysRevLett.109.102001](https://doi.org/10.1103/PhysRevLett.109.102001)

PACS numbers: 14.20.Gk, 13.60.Le

Symmetry arguments led Gell-Mann and Zweig to introduce the concept of quarks as constituents of mesons and baryons [1,2]. Later it was realized that quarks carry a new kind of charge, color, and are the sources of gluons transmitting the binding forces. A new theory evolved, quantum chromodynamics [3], which proved to be very successful for large momenta where the interaction becomes weaker. In the region of meson and baryon resonances, QCD resists any perturbative approach, and numerical calculations on a space-time lattice are necessary. It was only recently that the full baryon spectrum including physical quantum numbers was presented [4], even though unrealistically large quark masses had to be used. Qualitatively, these lattice results confirm the classic quark model calculations [5], whereas the agreement with a fully relativistic model is less convincing [6]. Yet the experimental mass spectrum exhibits some remarkable differences to these calculations. The $N(1440)$ resonance with spin parity $J^P = 1/2^+$ has a mass of 1440 MeV and

falls below its spin-parity partner $N(1535)$ with $J^P = 1/2^-$ while QCD on the lattice and quark model calculations predict the reverse. Also, above a mass of 1800 MeV, the number of observed resonances falls short of the number of predicted resonances.

Baryon resonances have very short lifetimes; hence, many resonances with different spin parities overlap; their properties have to be unfolded from data in partial wave analyses. Most partial wave analyses are done using πN elastic and charge exchange scattering, but photoproduction experiments offer the opportunity of analyzing resonances which were not accessible up to now. However, the number of independent observables necessary for a unique partial wave solution increases. Below the two-pion production threshold at $E_\gamma = 310$ MeV, the Watson theorem [7] relates the πN phases to those in the photoproduction of single pions. In this case the measurement of the differential cross section $d\sigma$ and of the photon beam asymmetry Σ is sufficient to determine precisely the s - and p -wave

multipoles ($l_\pi = 0, 1$), as well as the small ratio of electric quadrupole ($E2$) and magnetic dipole ($M1$) amplitudes in the $N \rightarrow \Delta(1232)$ transition [8,9]. Above the two-pion threshold, but still in the mass range where nucleon resonances carry only one unit of intrinsic orbital angular momentum, five experiments are sufficient to construct the spin-helicity structure of the photoproduction amplitude [10,11]. In general, the observation of eight polarization observables with high precision is required to construct the electric (E) and magnetic (M) multipoles governing the process [12,13].

In this Letter we report on a first measurement of the double-polarization observable G in the photoproduction of neutral pions off protons covering the second and third resonance region. Linearly polarized photons were produced by the scattering of a 3.2 GeV electron beam [14] off a diamond crystal [15], whereby a maximal polarization of 65% at 950 MeV and 59% at 1150 MeV for a second data set were reached. The photons then hit a butanol ($C_4H_{10}O$) target with longitudinally polarized protons [16], with a mean proton polarization of about 75%. The butanol target was replaced by a hydrogen or carbon target for background studies and for normalization. The incoming photons may produce a π^0 in the reaction

$$\vec{\gamma} \vec{p} \rightarrow p \pi^0. \quad (1)$$

For linearly polarized photons (with polarization p_γ) and protons (with polarization p_T), the number of events N at the polar angle θ_π due to reaction (1) as a function of the azimuthal angle ϕ_π can be written in the form

$$\frac{N(\phi_\pi, \theta_\pi)}{N_0(\theta_\pi)} = 1 - p_\gamma \Sigma_B \cos(2\phi_\pi) + p_\gamma p_T G_B \sin(2\phi_\pi), \quad (2)$$

where N_0 is given by averaging $N(\phi_\pi, \theta_\pi)$ over ϕ_π . The beam asymmetry Σ_B and the observable G_B for the butanol target are related to the corresponding quantities for scattering off free (f) protons, Σ and G , and bound (b) nucleons by

$$\Sigma_B = \frac{N_0^f \Sigma + N_0^b \Sigma_b}{N_0^f + N_0^b}; \quad G_B = \frac{N_0^f}{N_0^f + N_0^b} \cdot G. \quad (3)$$

The number of events in the denominator is the sum of the number of events where scattering took place off protons or a bound nucleon, $N_0 = N_0^f + N_0^b$. There is no contribution of bound nucleons to G_B since carbon and oxygen nuclei carry no polarization. The quantity $D = N_0^f / (N_0^f + N_0^b)$ is called the dilution factor and depends on the reaction and on the kinematical cuts performed. It is also possible to determine G without using the dilution factor by reversing the target polarization and regarding the difference $N^+(\phi_\pi, \theta_\pi) - N^-(\phi_\pi, \theta_\pi)$, given by $2N_0^f p_\gamma p_T G \sin(2\phi_\pi)$. A similar equation can be written for a change of the photon polarization plane by $\pm \pi/4$ [17].

Figure 1(a) shows the calorimeter setup. Neutral pions are reconstructed from their decay into two photons and a measurement of their energy and direction in CsI(Tl) and BaF₂ crystals enclosing the target hermetically. The proton direction is determined, assuming that it originated in the target center, from its hit in the surrounding three-layer scintillation fiber detector [18] or scintillation detectors in front of the crystals in the forward direction, and its hit in the CsI or BaF₂ crystals. In comparison to Ref. [19], two major instrumental changes have been introduced. The forward opening of the calorimeter is now covered by 90 additional CsI(Tl) crystals with a photomultiplier readout in the main calorimeter and 216 BaF₂ crystals, 2.1 m downstream of the target. The tagger is now mounted horizontally. Beam electrons not producing bremsstrahlung are now deflected to the left and are stopped in a beam dump well behind the detector system.

In the first step of the reconstruction, events due to reaction (1) are selected using a series of kinematical cuts. Two classes of events are retained, events with three hits in the calorimeters and events with two hits. Both hits of a two-hit event are assumed to be photons; their invariant mass is calculated and required to fall into a 3σ

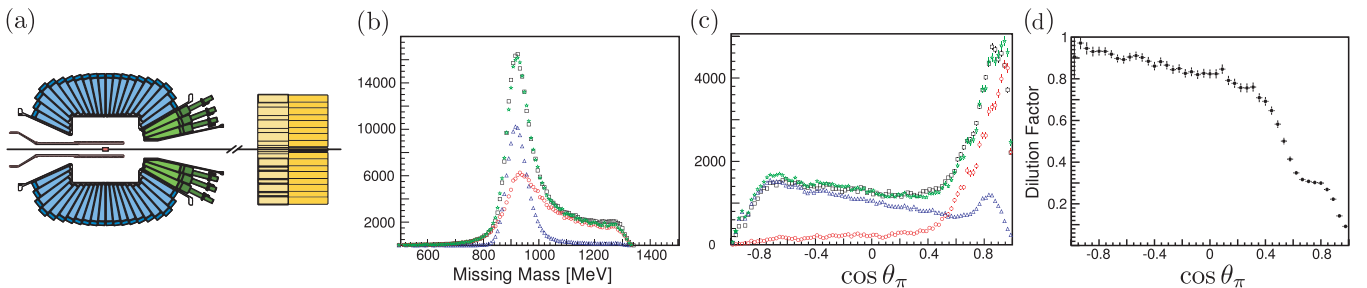


FIG. 1 (color). (a) The central part of the detector system. The CsI(Tl) crystals (blue and green) are read out via wavelength shifters and photodiodes or photomultipliers, BaF₂ crystals (yellow) in forward direction with photomultipliers. (b) The missing mass distribution, and (c) the π^0 angular distribution for reaction (1) for an incident photon energy of $E_\gamma = 1000 \pm 25$ MeV; butanol (black squares), hydrogen (blue triangle), carbon (red circle), and the sum of hydrogen and carbon data (green star). From these distributions, the dilution factor (d) is determined.

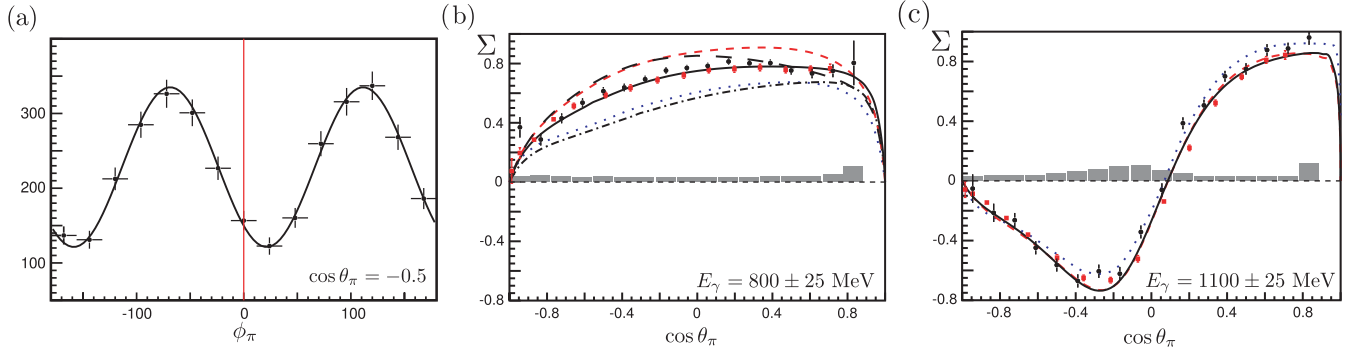


FIG. 2 (color). (a) A typical ϕ_π distribution with a fit using Eq. (2). (b, c) The beam asymmetry Σ as a function of $\cos\theta_\pi$ for $E_\gamma = 800$ MeV and for $E_\gamma = 1100$ MeV. Black dots show our data, red squares GRAAL data [20]. The curves represent predictions from different partial wave analyses. Solid (black) curve: BnGa [24]; dashed (red): SAID [22]; long-dashed (black): BnGa with E_{0^+} and E_{2^-} amplitudes from SAID; dotted (blue): MAID [23]; dashed-dotted (black): BnGa with E_{0^+} and E_{2^-} amplitudes from MAID. Gray area shows the systematic error due to interactions on nuclei and uncertainty in the photon polarization.

(± 25 MeV) window centered at the π^0 mass. The proton is assumed to be stopped in some material, but due to energy and momentum conservation, the proton momentum can be reconstructed. If there is a third hit, one pair of hits is assumed to be photons, and it is checked that the pair forms a π^0 , using again a $\pm 3\sigma$ window. The third hit has to match the direction of the proton momentum reconstructed as missing momentum. Matching is defined by a cone, $\pm 7^\circ$ in the azimuthal and polar angles. Finally, a time coincidence is required between the tagger hit and hits in one of the scintillation detectors or forward calorimeter crystals. Additionally all events are removed, if the calculated beam photon energy (under the assumption that the reaction occurred on a proton) falls below the tagging threshold. With these cuts the reconstruction efficiency for reaction (1) on free protons in the butanol target exceeds 60%.

Figure 1(b) shows the resulting distribution of missing masses for events passing the selection criteria, with butanol, carbon, or hydrogen as the target material. By proper scaling, the sum of the distributions from hydrogen and carbon reproduces very well the distribution obtained with the butanol target. The missing mass distributions show a peak at the proton mass and a tail due to events where an additional meson was produced but escaped detection. A final cut is now applied on the missing mass at $m_p \pm 50$ MeV. The resulting $\cos\theta_\pi$ distribution of these events is exhibited in Fig. 1(c). Again, the sum of the distributions from hydrogen and carbon match the distribution obtained with the butanol target; there is no new scaling factor involved.

For the double-polarization observable G the correction factor for reactions on nuclei is the dilution factor, displayed in Fig. 1(d). Due to the kinematic cuts, the dilution factor depends on both the photon energy E_γ and the π^0 scattering angle θ_π . For a backward π^0 , the proton momentum is high and therefore detected in the crystals with a high efficiency.

A typical distribution of the measured ϕ_π -dependent data yields with a fit using Eq. (2) is shown in Fig. 2(a). Obviously, there is a large $\cos 2\phi_\pi$ contribution but the data are not symmetric with respect to $\phi_\pi = 0$: there is a significant $\sin 2\phi_\pi$ contribution from which the desired observable G is deduced. Figures 2(b) and 2(c) show the beam asymmetry Σ extracted from this and other similar plots for two energy bins. The systematic errors due to reactions on nuclei are shown as gray bars. The new Σ data are in excellent agreement with earlier measurements of the GRAAL Collaboration [20].

The observable G is determined from Eq. (2), as well as by reversing the target polarization, or changing the photon polarization plane by $\pm\pi/4$. The results are consistent; their spread is used to determine the systematic errors. These include the systematic uncertainty in the dilution factor, errors due to background in $\cos\theta_\pi > 0.9$, the relative uncertainty in the target polarization of $\pm 2\%$, and the

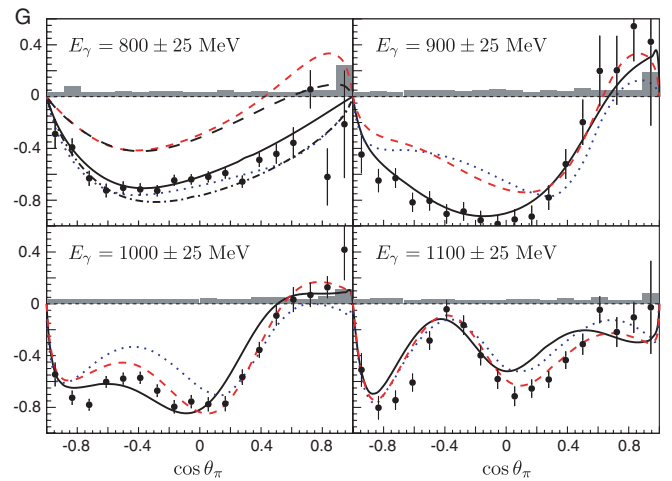


FIG. 3 (color). The polarization observable G as a function of $\cos\theta_\pi$ from $E_\gamma = 800$ MeV up to $E_\gamma = 1100$ MeV. Systematic errors are shown in gray bars. Curves: see Fig. 2.

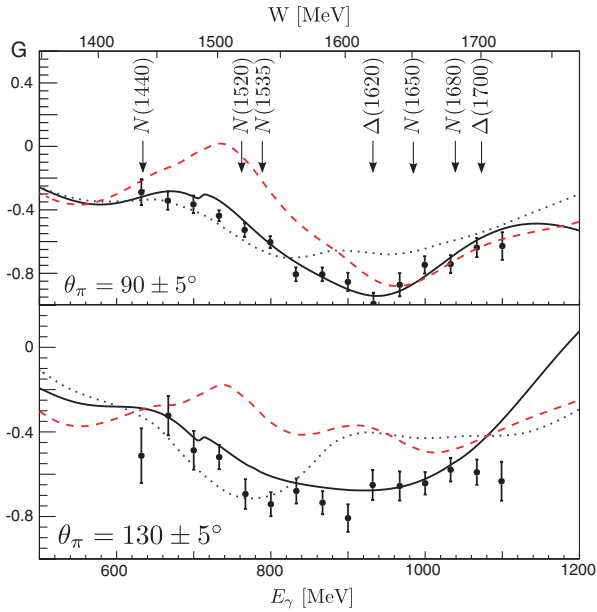


FIG. 4 (color). The double-polarization observable G as a function of energy for two selected bins in θ_π . Curves: see Fig. 2. For comparison the positions of several resonances are marked.

relative uncertainty in the photon polarization of $\pm 5\%$ [21]. Figure 3 shows the angular distribution of the polarization observable G for selected photon energy ranges. The error bars give the statistical errors; the systematic errors are shown as gray bars.

The new data on Σ and G are compared to the predictions from the SAID (SN11) [22], MAID [23], and BnGa [24] partial wave analyses. The results are surprising.

Already at rather low energies, in the region of the four-star resonances $N(1440)$, $N(1535)$, and $N(1520)$, very significant differences in the predictions can be observed (see Figs. 2 and 3). At 800 and 900 MeV, the SAID prediction is incompatible with the data on Σ and G , MAID disagrees with the data on Σ and on G at 900 MeV. At 1000 and 1100 MeV, BnGa, MAID, and SAID give a reasonable description, even though MAID is higher at 1000 MeV. These conclusions are supported by Fig. 4 where G is shown as a function of E_γ for two scattering angles and compared to the PWA predictions. At low energies, SAID deviates strongly from the data; in the 900–1000 MeV range, the consistency between the data and MAID or SAID predictions is poor. Above, none of the partial wave analyses reproduces the data.

We have studied possible reasons for the discrepant results. In this discussion, the two electric multipoles E_{0+} and E_{2-} play a leading role. If we replace the BnGa E_{0+} and E_{2-} multipoles by the corresponding SAID multipoles, we reproduce the SAID results for Σ and G over a wide energy range, and the same observation holds true for MAID. The reason for the deviation between the data and MAID and SAID is obviously traced to these two

TABLE I. Helicity amplitudes of low-lying negative parity N and Δ resonances contributing to the E_{0+} and E_{2-} multipoles (in $\text{GeV}^{-(1/2)}10^{-3}$).

E_{0+}	$N(1535)1/2^-$	$N(1650)1/2^-$	$\Delta(1620)1/2^-$	
Solution	$A^{1/2}$	$A^{1/2}$	$A^{1/2}$	
BG2011-02	105 ± 10	33 ± 7	52 ± 5	
MAID-2007	66	33	66	
SAID-2011	99 ± 2	65 ± 25	64 ± 2	
E_{2-}	$N(1520)3/2^-$	$\Delta(1700)3/2^-$		
Solution	$A^{1/2}$	$A^{3/2}$	$A^{1/2}$	$A^{3/2}$
BG2011-02	-22 ± 4	131 ± 10	160 ± 20	165 ± 25
MAID-2007	-27	161	226	210
SAID-2011	-16 ± 2	156 ± 2	109 ± 4	84 ± 2

multipoles. All other multipoles can be exchanged without a large impact.

Resonances with no angular momentum between the proton and π^0 ($l_\pi = 0$) contribute to the E_{0+} multipole which is sensitive to the $N(1535)$, $\Delta(1620)$ and $N(1650)$ resonances. The resonances $N(1520)$ and $\Delta(1700)$ with $l_\pi = 2$ and total spin $J = 3/2$ contribute to the E_{2-} multipole. Indeed, the three partial wave analyses BnGa, MAID, and SAID give significantly different helicity amplitudes for these resonances, in particular for the $A_{1/2}$ amplitude of $N(1535)$ and for $A_{3/2}$ of $N(1520)$ (see Table I).

In the medium energy region, in the third resonance region, the $\gamma p \rightarrow p\pi^0$ cross section is dominated by the $J^P = 5/2^+$ $N(1680)$ resonance. In this regime, there is good agreement between the three predictions. The properties of this resonance are obviously well defined: for the leading $A_{3/2}$ helicity amplitude, BnGa finds 135 ± 6 , MAID 134, and SAID 141 ± 3 (in $\text{GeV}^{-(1/2)}10^{-3}$).

In the high energy region, increasing differences between the predictions can be observed for some angles. This is the so-called fourth resonance region where many resonances exist with questionable evidence for their existence and, if they exist at all, with at least poorly defined properties. New data on G in this energy region will help to disentangle the spectrum of nucleon resonances [21].

Summarizing, we have reported the first measurement of the double-polarization observable G in the reaction $\vec{\gamma} \vec{p} \rightarrow p\pi^0$ in a wide range of energies and covering the full solid angle. The new data on G resolve the discrepant results on the helicity amplitudes of low-lying four-star nucleon resonances obtained from BnGa, MAID, and SAID and are an important step towards a complete database which will define unambiguously the nucleon excitation spectrum.

We thank the technical staff of ELSA and the participating institutions for their invaluable contributions to the success of the experiment. We acknowledge support from the Deutsche Forschungsgemeinschaft (SFB/TR16) and Schweizerischer Nationalfonds.

- [1] M. Gell-Mann, *Phys. Rev.* **125**, 1067 (1962).
- [2] G. Zweig, Report No. CERN-TH-401 1964.
- [3] H. Fritzsch and P. Minkowski, *Nuovo Cimento A* **30**, 393 (1975).
- [4] R. G. Edwards, J. J. Dudek, D. G. Richards, and S. J. Wallace, *Phys. Rev. D* **84**, 074508 (2011).
- [5] N. Isgur and G. Karl, *Phys. Rev. D* **18**, 4187 (1978).
- [6] U. Löring, B. Ch. Metsch, and H. R. Petry, *Eur. Phys. J. A* **10**, 395 (2001).
- [7] K. M. Watson, *Phys. Rev.* **95**, 228 (1954).
- [8] R. Beck *et al.*, *Phys. Rev. Lett.* **78**, 606 (1997).
- [9] G. Blanpied *et al.*, *Phys. Rev. Lett.* **79**, 4337 (1997).
- [10] A. S. Omelaenko, *Yad. Fiz.* **34**, 730 (1981).
- [11] Y. Wunderlich, Diploma thesis, Univ. Bonn, 2012.
- [12] W.-T. Chiang and F. Tabakin, *Phys. Rev. C* **55**, 2054 (1997).
- [13] A. M. Sandorfi, S. Hoblit, H. Kamano, and T.-S. H. Lee, *J. Phys. G* **38**, 053001 (2011).
- [14] W. Hillert, *Eur. Phys. J. A* **28S1**, 139 (2006).
- [15] D. Elsner *et al.*, *Eur. Phys. J. A* **39**, 373 (2009).
- [16] H. Dutz *et al.*, *Phys. Rev. Lett.* **93**, 032003 (2004).
- [17] A. Thiel, Ph.D thesis, Universität Bonn, 2012.
- [18] G. Suft, G. Anton, R. Bogendörfer, A. Ehmans, A. Fösel, J. Höbl, H. Kalinowsky, C. Küppersbusch, and D. Walther, *Nucl. Instrum. Methods Phys. Res., Sect. A* **538**, 416 (2005).
- [19] V. Crede *et al.*, *Phys. Rev. C* **84**, 055203 (2011).
- [20] O. Bartalini *et al.*, *Eur. Phys. J. A* **26**, 399 (2005).
- [21] A. Thiel, H. Eberhardt *et al.* (to be published).
- [22] R. Workman, W. J. Briscoe, M. W. Paris, and I. I. Strakovsky, *Phys. Rev. C* **85**, 025201 (2012).
- [23] D. Drechsel, O. Hanstein, S. S. Kamalov, and L. Tiator, *Nucl. Phys. A* **645**, 145 (1999).
- [24] A. V. Anisovich, R. Beck, E. Klempt, V. A. Nikonov, A. V. Sarantsev, and U. Thoma, *Eur. Phys. J. A* **48**, 15 (2012).